water

MDPI

Article

2D and 3D Numerical Simulation of Dam-Break Flooding: A Case Study of the Tuzluca Dam, Turkey

Cagri Akgun [1,*], Salim Serkan Nas [2] and Akin Uslu [2]

[1] Igdir Vocational School of Higher Education, Igdir University, 76000 Igdir, Turkey
[2] Civil Engineering Department, Gumushane University, 29100 Gumushane, Turkey; serkannas@gmail.com (S.S.N.); usluakin@hotmail.com (A.U.)
* Correspondence: cagriakgun2063@gmail.com

Abstract: Unlike river floods, floods caused by dam breaks occur much more abruptly and at higher water velocities. The failure of a dam due to any reason can pose a significant threat to settlements in the downstream area due to the high volume of water in its reservoir. In this case study, 2D and 3D numerical failure simulations of Tuzluca Dam, to be built in the Igdir province of Turkey, was performed using the Flow3D Hydro software. The Shallow Water and Reynolds-Averaged Navier-Stokes (RANS) equations were used to simulate flood propagation. In the numerical models, RNG k-ε was chosen as the turbulence model. In the analyses carried out under different scenarios, it was observed that in both methods (2D and 3D), significant flood depths would occur in two downstream village settlements. Within the scope of the study, the mortality rates in different dam-break scenarios of the Tuzluca Dam were also investigated. It has been observed that the dam failure time and breach geometry have a significant impact on the flood propagation and the loss of life in settlements. Additionally, a dam-break experiment in literature dam-break experiment was numerically solved using the Flow3D Hydro software to validate the numerical model, and a satisfactory harmony was observed between the experimental results and the numerical models. Although the 3D analysis provided a more accurate representation of the experimental results, it took approximately 20 times longer to complete the dam failure simulation in the case study compared to the 2D model. As a result, it has been determined that for comprehensive studies such as those of dam failures, 2D analyses may be more practical, while for smaller-scale scenarios or situations requiring greater precision, 3D modelling is appropriate.

Keywords: dam-break modelling; dam overtopping; flood propagation; Flow3D; validation of numerical models

Citation: Akgun, C.; Nas, S.S.; Uslu, A. 2D and 3D Numerical Simulation of Dam-Break Flooding: A Case Study of the Tuzluca Dam, Turkey. *Water* **2023**, *15*, 3622. https://doi.org/10.3390/w15203622

Academic Editor: Paolo Mignosa

Received: 8 September 2023
Revised: 9 October 2023
Accepted: 12 October 2023
Published: 16 October 2023

1. Introduction

Dams, constructed to retain flowing water in river valleys, have been utilized for centuries to meet humanity's water needs. The collapse of a dam for any reason results in floods occurring at much more abrupt and rapid water velocities compared to river floods due to the high water mass in its reservoir. Therefore, dam collapses represent low-probability but high-risk disaster events [1–3].

Historical dam breaks have shown a high occurrence of casualties and property losses. In 1979, the collapse of the Machuchu-2 Dam in India resulted in 5000 deaths, while the collapse of the Val De Stava Dam in Italy in 1985 caused the loss of 286 lives. Similarly, the collapse of the Patel Dam in Kenya in 2018 resulted in 47 deaths, and the collapse of the Brumadinho Dam in Brazil in 2019 claimed the lives of 270 people, providing recent concrete examples in this regard [4,5].

Dam breaks can occur due to various factors, both internal and external. Research has shown that factors such as overtopping, piping (internal erosion), earthquakes, seepage, and structural issues can lead to dam breaks [6,7]. According to the data from the

International Commission on Large Dams (ICOLD), 44% of the past dam breaks occurred due to overtopping, while 34% occurred due to piping [8]. There has been no dam failure in Turkey, the study region, and only in 2012, a flood occurred in the construction area as a result of the rupture of the derivation tunnel cover during the construction of a dam in Adana province. Regardless of the cause, all dam breaks begin with the formation of a breach, which grows and leads to the break of the dam [2]. In the case of dam failure caused by overtopping, breach initiation typically occurs in the dam crest and tends to grow downward, often assuming a trapezoidal shape. On the other hand, in the case of failure caused by piping, commonly observed in embankment dams, breaches start at any location in the dam body and grow in both the transverse and longitudinal directions, forming a trapezoidal or rectangular shape [9–11].

Studies on dam failure provide valuable information for the development of early warning systems and evacuation plans in downstream areas. Conducting possible dam-break simulations and establishing early warning systems contribute to preventing or mitigating disasters for existing and planned dams [3,12]. In recent years, many studies have been carried out on flood control and prediction methods using remote sensing and GIS technology. Li et al. [13], in their study, analyzed the public's awareness of the debris flow using 3D remote sensing methods and made suggestions to improve people's behavior concerning this issue. Liu et al. [14] stated that monitoring urban water resources using remote sensing and geostatistical technologies will benefit flood control. Oborie and Rowland [15] developed an impact flood prediction method based on hydrological and morphological data using remote sensing and GIS techniques for river basins.

The problem of dam breaks has been the subject of numerous studies focusing on statistical, experimental, and numerical solutions. Researchers such as MacDonald and Langridge-Monopolis [9], Von Thun and Gillette [16], Froehlich [6,17], and Xu and Zhang [18] have developed empirical formulas based on statistical analysis of past dam breaks with reliable data to estimate parameters such as the average breach width, peak discharge, and failure time for potential dam breaks.

Experimental studies on dam breaks have been used not only to focus on hydraulic parameters such as the breach geometry, time-varying outflow hydrograph, flow velocity, and flow depths, but also to validate numerical simulations related to dam breaks [19,20]. Bella et al. [21] experimentally investigated the case of a sudden dam break in straight and curved horizontal channels. They monitored the pointwise variations of the water levels at five different points in the downstream region for conditions of curved and smooth channel beds. Lauber and Hager [22] conducted an experimental dam-break study in a rectangular smooth channel and compared the results with the analytical solutions developed by Ritter [23] for dam breaks. Soares-Frazao [24] performed an experimental dam-break test in a rectangular horizontal channel, with a triangular bottom sill placed in the downstream region, to examine the behavior of the flood wave during sudden changes in the slope using video cameras and level gauges. Hui et al. [25] experimentally investigated sudden dam breaks in a horizontal rectangular channel under different reservoir depths and wet and dry downstream conditions. They compared the obtained results with the analytical methods developed by Stoker [26], Lin et al. [27], and Ritter [23].

Many studies have used the shallow water equations, also known as the Saint-Venant equations, for the numerical solution of the dam-break problem [28]. Albano et al. [29] conducted 1D and 2D dam failure analyses for the San Giuliano and Gleno Dams using the Saint-Venant equations and developed a Geographic Information System-based flood mapping method for masonry arch and gravity dams. Riha et al. [30] examined the flood propagation effect of multiple dam failures by performing 2D dam failure analysis of three dams on the Cižina River (Czech Republic) using the HECRAS v. 5.0.7 software. Psomiadis et al. [31] performed 2D failure analysis of the Bramianos dam using two different surface models; the dam failure analyses were performed using a digital elevation model (DEM) obtained from reliable satellite photographs and a digital surface model (DSM) obtained with an unmanned aerial vehicle (UAV), and the results were compared. Bello et al. [32]

used the HEC-RAS and McBreach v 5.0.7 software to conduct dam failure analysis of the Chacrillas dam. Sensitivity analyses performed in the study revealed that the most significant factor influencing the maximum discharge after failure is the failure time.

Although the Saint-Venant equations provide significant advantages in terms of the solution time and ease, they have important limitations, such as neglecting vertical acceleration and the dominance of hydrostatic pressure conditions in the flow; that is, the water depth is considered to have a small ratio compared to the length in the horizontal direction. In these cases, the flow is represented in 1 or 2 dimensions. However, a real dam break is a fluid dynamics problem where the 3-dimensional components of velocity and acceleration are active, sudden topographic changes can occur, and hydrostatic pressure conditions do not dominate [6,33,34]. The complexity of the hydraulic components and the wide extent of flood impact in a real dam break require long computation times and computers with a high processing power for numerical solutions. Therefore, a significant portion of the 3D dam-break studies in the literature have been conducted by creating and solving a flood wave in small-scale horizontal channels using numerical models. Larocque et al. [35] solved a previously published dam failure experiment numerically in 3D using the LES and k-e turbulence models. Robb and Vasquez [36] numerically solved two previously published experimental studies. Within the scope of the study, the results of the experiments solved in 2D using the Telemac-2D software and in 3D using the Flow3D and Openfoam software were compared. Tahershamsi et al. [37] investigated the effect of the breach ratio and reservoir geometry on the peak discharge in dam failure using both experimental and numerical methods. Through 3D analyses conducted using the Ansys Fluent v. 6.3.26 software, they developed empirical formulas based on the reservoir shape factor and dam breach ratio. Franco et al. [38] conducted numerical analysis of the 1958 Lituya Bay tsunami event. In the 3D analyses performed using the Flow3D software, they examined the propagation of the flood wave caused by the tsunami and compared it with historical data. Kocaman et al. [39] numerically simulated their laboratory-developed dam-break experiment using the Flow3D software. The results of the numerical simulations conducted using the Shallow Water Equations (SWE) and Reynolds-Averaged Navier-Stokes (RANS) equations were compared. Additionally, within the scope of their study, the experiment was repeated for different tailwater depths to investigate the effect of tailwater on flood propagation.

When reviewing the literature, it is observed that due to the long solution times associated with 3D dam-break analyses, dam-break analyses at the actual topographical scale are performed in 1D and 2D. Furthermore, for similar reasons, studies comparing 2D and 3D analyses in dam-break scenarios have been conducted in scaled-down experimental setups.

In this case study, dam-break analyses were conducted at a real dam topography scale, considering the gaps in the literature, using 2D Shallow Water Equations (SWE) and 3D Navier-Stokes Equations (RANS). The study area was selected as the planned Tuzluca Dam in the eastern-most province of Turkey; namely, Iğdır. The suitability of 3D modeling in large-scale topographies was explored by comparing the results of the analyses conducted using the two different methods. Furthermore, the impact of different breach geometries, failure modes, and failure times on flood propagation was investigated by implementing three different scenarios. The risk situations and possible loss of life in settlements in the downstream area were evaluated in the conducted analyses. Another significance of the study is that the selected Tuzluca Dam is still in the planning phase, so the findings and risks obtained in the research can provide some revision opportunities to decision-makers regarding the project.

2. Materials and Methods

2.1. Study Area and Dam Characteristics

Tuzluca Dam, which has been included in the investment program by the public, and the necessary plans and projects have been prepared. It is planned to be built on the 40°07′52″ N and 43°38′12″ E coordinate lines on the Aras River, which forms the Turkey–Armenia border in Igdir, Turkey. The location map is given in Figure 1, below.

Figure 1. Location map of the Tuzluca Dam.

The study area covers a large area of 101.5 km^2. The settlements of Halimcan, Halikisla, Turabi, Surmeli, and Calpala on the Turkish border, and the settlements of Bagaran and Yervandashat on the Armenian border are potential at-risk settlements in the downstream region of the dam.

The Tuzluca Dam is planned to be a rock-fill dam with a height of 45 m. The dam, with a reservoir capacity of 265 million m^3, is designed to generate hydroelectric power, with an installed capacity of 20 MW, while also providing irrigation benefits. Three villages will be submerged by the reservoir upon the construction of the dam. The cross-section of the dam body is shown in Figure 2, below.

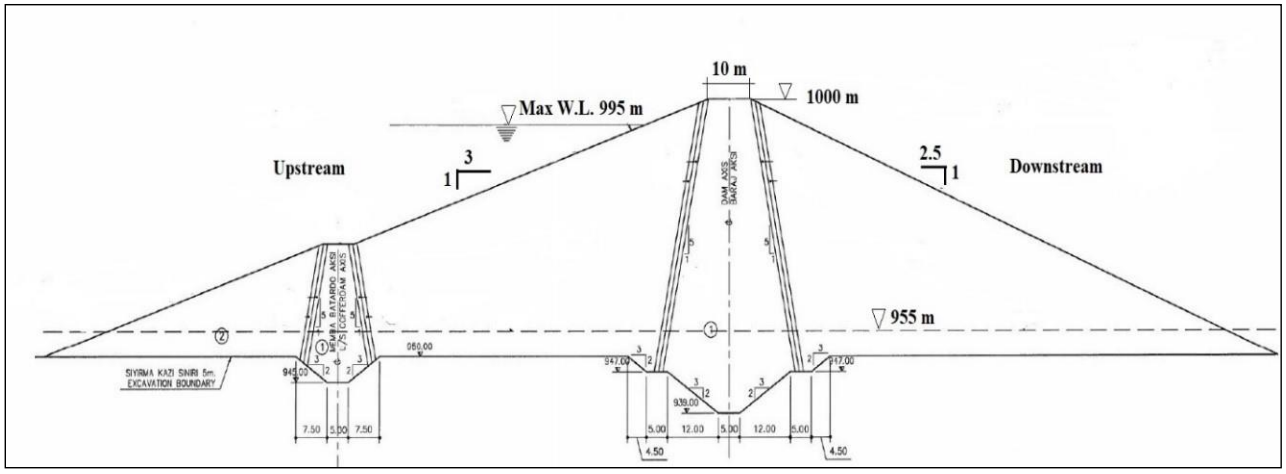

Figure 2. Section of Dam Body [40].

2.2. Geometric Data

In hydraulic modelling, accurately representing the geometry of the study area is an essential requirement; particularly in extensive studies such as dam breaches, obtaining topographic data through remote sensing methods provides significant convenience to users [41,42].

In this study, a digital elevation model (DEM) with a resolution of 12.5 m from the ALOS satellite was used to represent the topographic conditions. The ALOS satellite, launched by the Japan Aerospace Exploration Agency (JAXA) in 2006, was developed to contribute to various studies such as cartography, resource exploration, disaster monitoring, and environmental change analysis [43]. The reliability of the DEM data from the ALOS satellite has been tested for flood risk analysis in various studies and is considered to be successful [44,45]. The DEM data for the study area were converted to the Stereolithography (STL) format using the Global Mapper v. 24.0 software and transferred to the Flow3D software.

2.3. Estimation of Dam Breach Parameters

One of the most significant uncertainties in dam failure analyses is the estimation of the breach parameters. In this context, calculations were made using the methods developed by MacDonald and Langridge-Monopolis [9], Bureau of Reclamation [46], Von Thun and Gillette [16], Froehlich [6,17], and Xu and Zhang [18] to calculate the breach dimensions and failure time. The breach parameters calculated according to the relevant methods are presented in Table 1.

Table 1. Calculated breach parameters.

Method	B_t (m)		B_{ave} (m)		B_b (m)		T_f (h)	
	O	P	O	P	O	P	O	P
MacDonald and Langridge-Monopolis [9]	341	<u>224</u>			161	<u>224</u>	3	
Bureu of Reclamation [46]			135				1.5	
Von Thun and Gillette [16]			167				<u>1</u>	
Froehlich [17]			258	184			2.4	
Froehlich [6]			218	156			2	
Xu and Zhang [18]	<u>380</u>	222	287	168	<u>217</u>	87	2.4	2.3

Note(s): The values used in the simulations are underlined. B_t: breach top width, B_{ave}: breach average width, B_b: breach bottom width, T_f: failure time, O: overtopping, P: piping.

When comparing the methods in the literature, it is observed that the most unfavorable conditions in terms of the breach dimensions in overtopping scenarios are obtained using the method proposed by Xu and Zhang [18], while the methods proposed by Von Thun and Gillette [16] are found to be particularly unfavorable in the case of failure time. Consequently, the Xu and Zhang [18] method was employed for the overtopping scenarios. As the rectangular breach condition for dam failures caused by piping can only be applied using the MacDonald and Langridge-Monopolis [9] method, the MacDonald and Langridge-Monopolis [9] method was chosen to examine different breach geometries in the piping scenario. In the 3rd scenario, the effect of reducing the failure time to half an hour on flood propagation was investigated, considering breach dimensions calculated using the method proposed by Xu and Zhang [18]. Information about the scenarios is visualized in Figure 3.

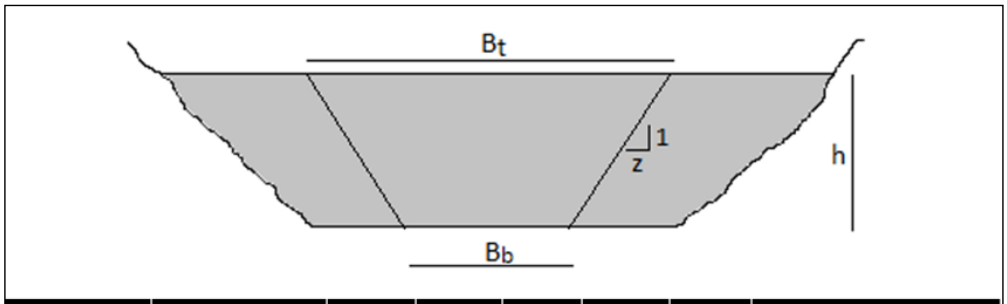

	Failure Type	Bt (m)	Bb (m)	h (m)	z	t (h)	Method
Scenario 1	Overtopping	380	217	45	1.8	1	Xu and Zhang
Scenario 2	Overtopping	380	217	45	1.8	0.5	Xu and Zhang
Scenario 3	Piping	224	224	45	0	1	MacDonald and Langridge-Monopolis

Figure 3. Information regarding dam failure scenarios in Flow3D.

2.4. Flow3D Numeric Model

In this study, the possible failure simulation of the Tuzluca Dam was numerically modelled as 2D and 3D using the Flow3D software to investigate the impact of flooding on downstream settlements under different scenarios. Flow3D is a computational fluid dynamics (CFD) software specifically developed to solve fluid flow equations [47].

The software utilizes the Volume of Fluid (VOF) method to track the free surface of the fluid in the calculation grids and employs the Fractional Area-Volume Obstacle Representation (FAVOR) algorithm to define solid objects [33,48]. In this study, the Renormalized Group (RNG) k-ε model, widely used in the dam-break analyses in the literature and validated in many studies, was selected as the turbulence model. This model can accurately model turbulent flow conditions with both high and low Reynolds numbers [49–55].

Flow3D offers two different approaches to deal with surface roughness. In the first approach, the surface roughness is obtained by pre-processing the solid object model (STL file) of the topography using the FAVOR technique. Additionally, due to the fact that the mesh blocks created do not perfectly conform to the terrain surface, there is also roughness depending on the angle formed. As a second option, Flow3D provides the possibility to define custom surface roughness. This feature can be used in cases where additional roughness is introduced in the topography, such as the presence of vegetation [38]. In the simulations conducted within the scope of the study, a roughness value of 1 m was used in areas with vegetation. In other areas, this coefficient was set to 0.

The Flow3D software uses artificial probes to detect the physical properties of water waves at any given point. In this study, probes were assigned to 7 settlements at risk of flooding to examine the water depths in post-failure settlements (Figure 4).

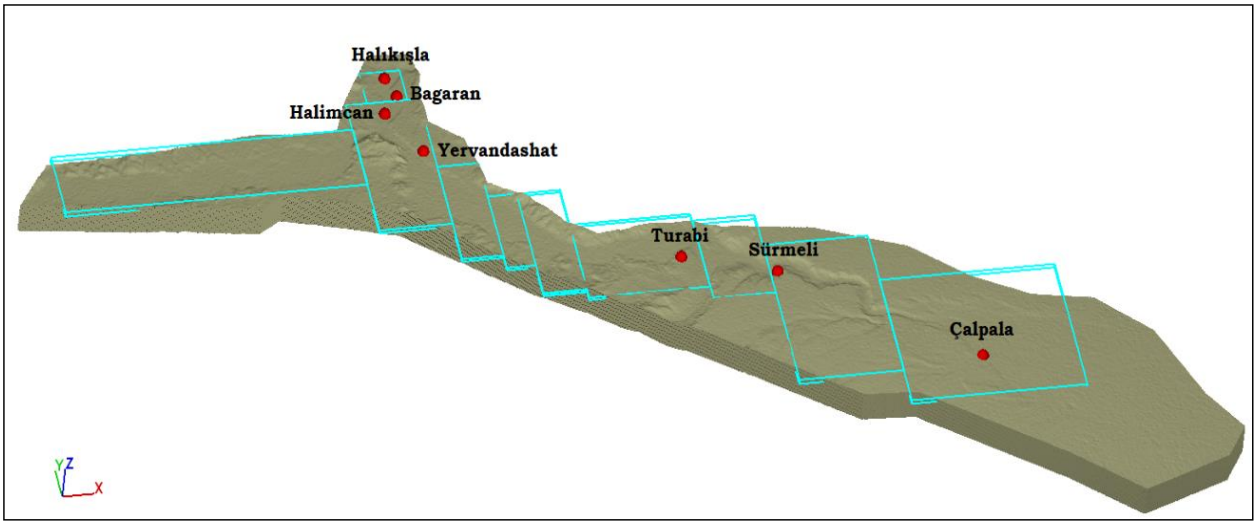

Figure 4. Display of topography, mesh blocks and probes in Flow3D software.

The numerical model was solved using two different methods—the 2D Shallow Water equation and 3D Navier Stokes equations—and the results were compared.

2.4.1. Two-Dimensional Shallow Water Equations

2D dam failure analyses can be performed by activating the Shallow Water model in the Flow3D software. The solution equation of the Shallow Water model is given below.

$$\frac{\partial V_f F}{\partial t} + \frac{\partial u A_x F}{\partial x} + \frac{\partial v A_y F}{\partial y} = 0 \quad (1)$$

In these equations, u represents the velocity of the fluid in the x direction, A_x represents the area occupied by the fluid in the calculation cell in the x direction, V_f represents the volume occupied by the fluid in the calculation cell, v represents the velocity of the fluid in the y direction, A_y represents the area occupied by the fluid in the calculation cell in the y direction, and F represents the fluid depth.

In the 2D analysis, the mesh size was determined as 10 m × 10 m in the areas where settlements with the risk of casualties are located, and 20 m × 20 m in the other regions. A total of 606,248 rectangular mesh cells were created in 10 different mesh blocks.

2.4.2. Three-Dimensional Reynolds-Averaged Navier-Stokes Equations

Flow3D can solve the three-dimensional motion equations (Reynolds-averaged Navier-Stokes equations) and continuity equations simultaneously using the finite volume method.

$$\frac{\partial}{\partial x_i}(u_i A_i) = 0 \quad (2)$$

$$\frac{\partial u_i}{\partial t} + \frac{1}{V_f}\left(u_j A_j \frac{\partial u_i}{\partial x_j}\right) = -\frac{1}{\rho}\frac{\partial p}{\partial x_i} + G_i + f_i \quad (3)$$

In these equations, u_i represents the velocity of the fluid in the i direction, A_i represents the area occupied by the fluid in the calculation cell in the i direction, V_f represents the volume occupied by the fluid in the calculation cell, p represents the pressure, G_i represents the gravitational acceleration in the i direction, and f_i represents the turbulence stresses in the i direction [49].

In the 3D analysis, the mesh size was determined as 10 m × 10 m × 1 m in the areas where settlements with the risk of casualties are located, and 20 m × 20 m × 1 m in the other regions. A total of 14,823,728 rectangular mesh cells were created in 10 different mesh

blocks. The general characteristics of the 2D and 3D numerical model are summarized in Table 2. All scenarios were modelled with a water level of 1000 m (dam crest elevation) along the dam axis at the moment of break. The visualization of the numerical model with the reservoir is shown in Figure 5.

Table 2. Characteristics of the numerical model in Flow3D.

General	Finish time	1. Scenario 7200 s 2. Scenario 4700 s 3. Scenario 6500 s
	Simulation units	SI
	Flow Mode	Incompressible
Physics	Gravity z component	-9.81 m/sn^2
	Turbulence model	RNG k-ε
Fluids	Material	Water at 20 °C
	Density	1000 kg/m^3
Meshing and Geometry	Size of cells	10 m × 10 m; 20 m × 20 m
	Total number of real cells *	606,248; 14,823,728
	Mesh type	Cartesian
	Boundary conditions **	X_{min} = Wall, Symmetry X_{max} = Symmetry, Outflow Y_{min} * = Wall Y_{max} * = Wall Z_{min} = Wall Z_{max} = Outflow

Note(s): * The total number of meshes in 2D analysis is 606,248. Because 1 m mesh size is used in the *z* direction in 3D analysis, the total number of meshes is 14,823,728. ** In the first mesh block, the boundary condition X_{min} = Wall was applied, while in the other mesh blocks, the boundary condition X_{min} = Symmetry was applied to ensure continuity. In the last mesh block, the boundary condition X_{max} = Outflow was applied, while in the other mesh blocks, the boundary condition X_{max} = Symmetry was applied.

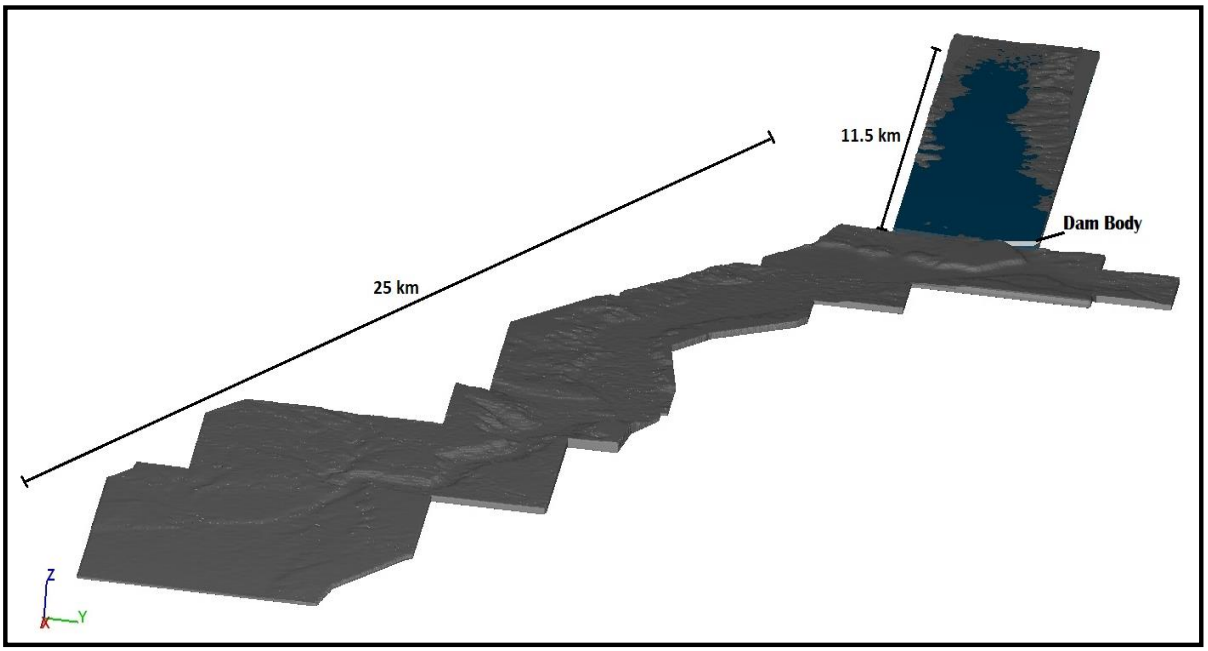

Figure 5. 3D solid model of the Tuzluca Dam and reservoir in Flow3D.

The failure of an actual embankment dam occurs gradually due to the time-dependent growth of a breach [11,19]. In the analysis conducted in this study, the breach formation was modelled by introducing moving parts into the system. The Flow3D software allow the definition of moving body elements along the dam axis to create the dam body. These

parts were assigned various speeds in the vertical and horizontal directions to achieve the desired final breach width and opening time for each scenario. When the simulations were performed, visualizations of the dam body and water flow were obtained for both trapezoidal and rectangular breach geometries, as shown in Figure 6.

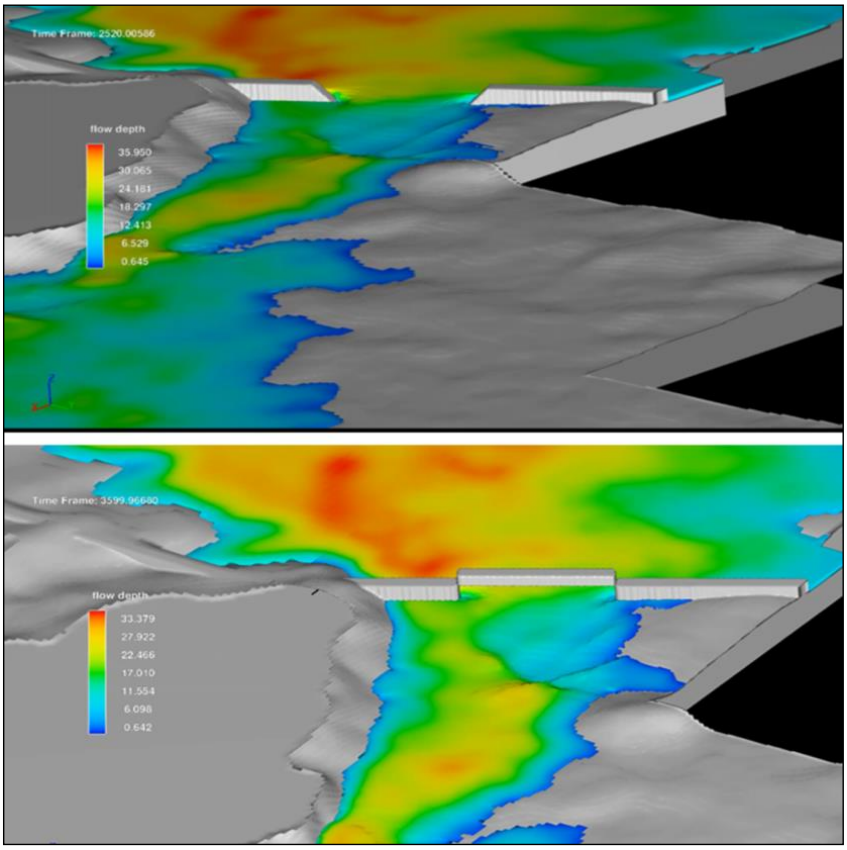

Figure 6. Trapezoidal and rectangular breach formations in simulations in Flow3D.

2.5. Model Validation

Laboratory experiments are often used to validate numerical models of dam breaks [20]. In this study, the dam-break experiment conducted by Soares-Frazao [24] was numerically solved in the Flow3D software to validate the numerical model, and the results were compared. The experiment consisted of a rectangular channel with closed ends, measuring 0.5 m in width and 5.6 m in length. By placing a vertical gate at a distance of 2.39 m from the starting point, a reservoir area with a height of 0.111 m and a length of 2.39 m was created. In addition, there is a triangular bottom sill, with a crest height of 0.065 m and a side slope of 0.14, located 1.61 m downstream of the dam (gate). There is water at a depth of 0.02 m in the section after the sill (Figure 7). A dam failure experiment was performed by removing the gate, and the water depths were measured using a three level-gauge and a digital camera. The locations of the level gauge are given in Table 3.

Table 3. Position of level gauges of Soares-Frazao (2007).

Level Gauge	x (m)	y (m)
G1	5.575	0.25
G2	4.925	0.25
G3	3.935	0.25

Note(s): The dam gate is located at $x = 0$.

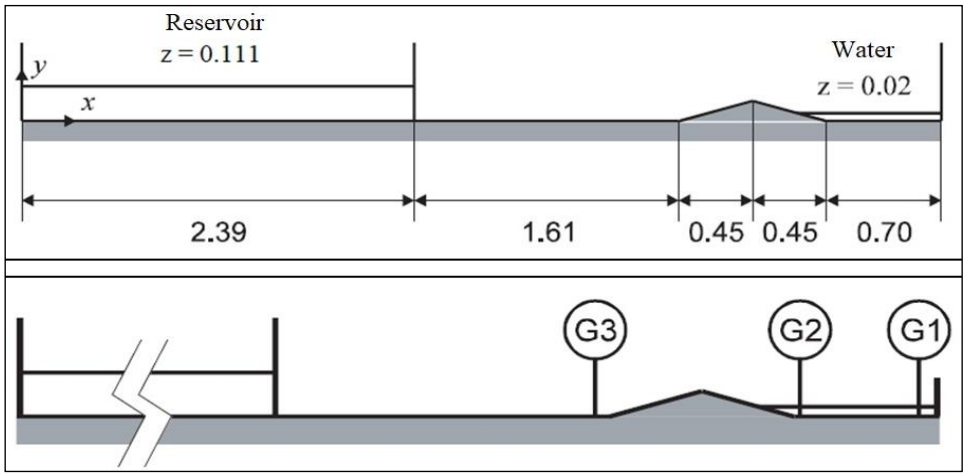

Figure 7. Experimental model of Soares-Frazao (2007) and level gauges.

The experimental model was set up in the Flow3D software using the same measurements (Figure 8.) Probe points were assigned to the positions given in Table 3 to compare the numerical model results with the experimental data.

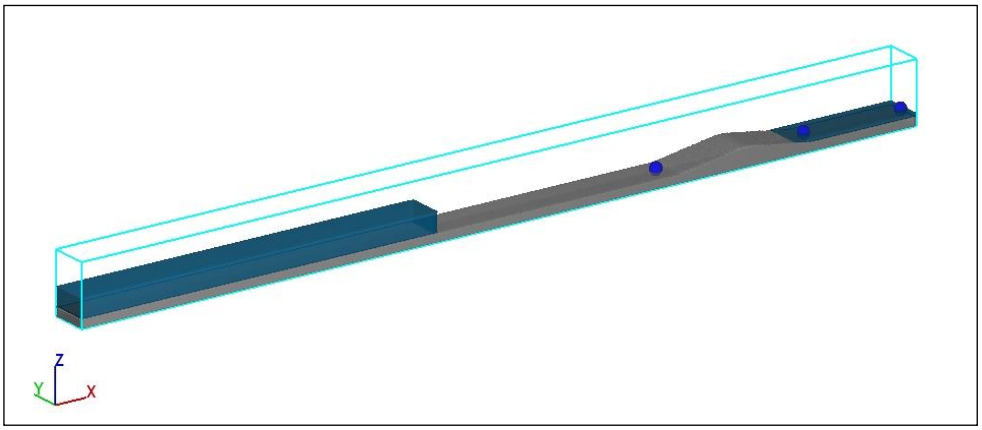

Figure 8. Soares-Frazao (2007) experimental model created in Flow3D software.

In the numerical simulation, the grid cells were selected with a resolution of 0.02 m in the x and y directions for the 2D analysis. It was selected to be 0.02 m × 0.02 m × 0.005 m for the 3D analysis. A total of 7000 and 254,800 mesh cells were used in the 2D and 3D analyses, respectively. The RNG k-ε turbulence model was selected for the simulations. The 45-s experimental data, which measured the changes in the water level over time at the G1, G2, and G3 points, were compared with the measurement results at the G1, G2, and G3 probe points in the numerical simulations.

3. Results and Discussion

Three different simulations were carried out for three scenarios determined over two different types of failure (overtopping, piping), different breach sizes, and different failure times (Figure 3). The analyses were conducted using a computer equipped with an Intel i7, 6-core processor, and 16 GB of RAM. While the average solution time for each scenario was 18 h in the 2D analysis, this time was 15 days in the 3D analysis.

The orthogonal form of the study area for the 2D analyses in the Flow3D software provides more precise results. For this reason, the topography is represented by orthogonal mesh blocks in the 2D analysis.

The changes in the flood propagation and flow depths over time for each scenario in the 2D analyses are shown in the Figures 9–11 below.

When examining the flood propagation simulations for each scenario, it can be observed that in Scenario 2, where the dam-break time is shorter, as expected, the flood propagation velocity is higher. In Scenario 3, where the failure occurs due to piping and has a smaller breach geometry, the flood propagation velocity is the lowest.

To further analyze the arrival times of a flood and the effects of flood propagation on the at-risk settlements, probe points were assigned to seven settlements. According to the simulation results, it was observed that only the Halimcan and Surmeli villages were affected by the flood wave. As the other villages were located in higher areas, only agricultural lands were affected. The flood depths in the village settlements for each scenario are shown in Figure 12.

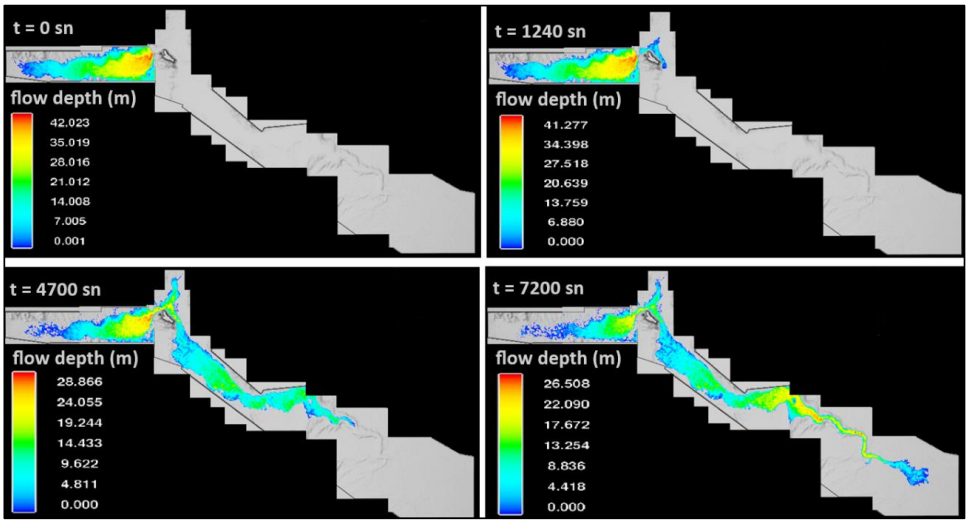

Figure 9. Flood depths and propagation over time for Scenario 1 in 2D analyses in Flow3D.

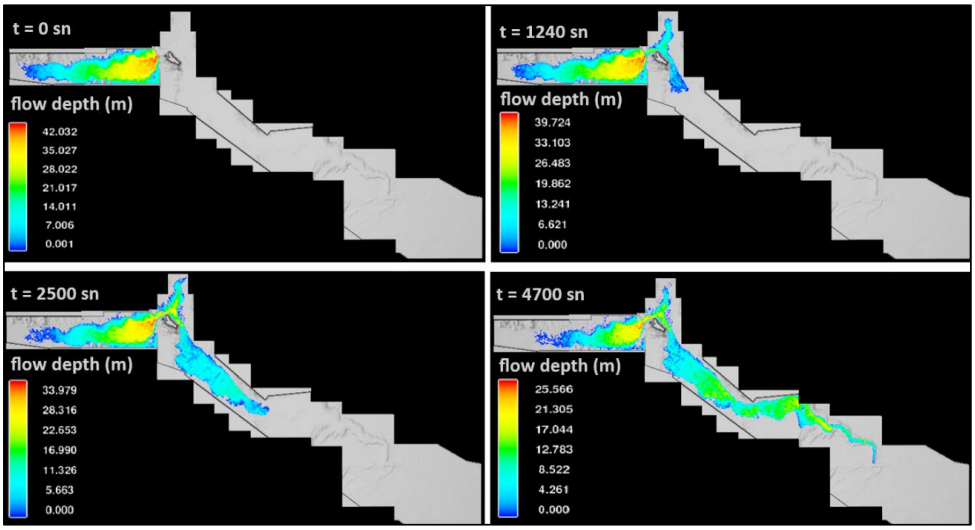

Figure 10. Flood depths and propagation over time for Scenario 2 in 2D analyses in Flow3D.

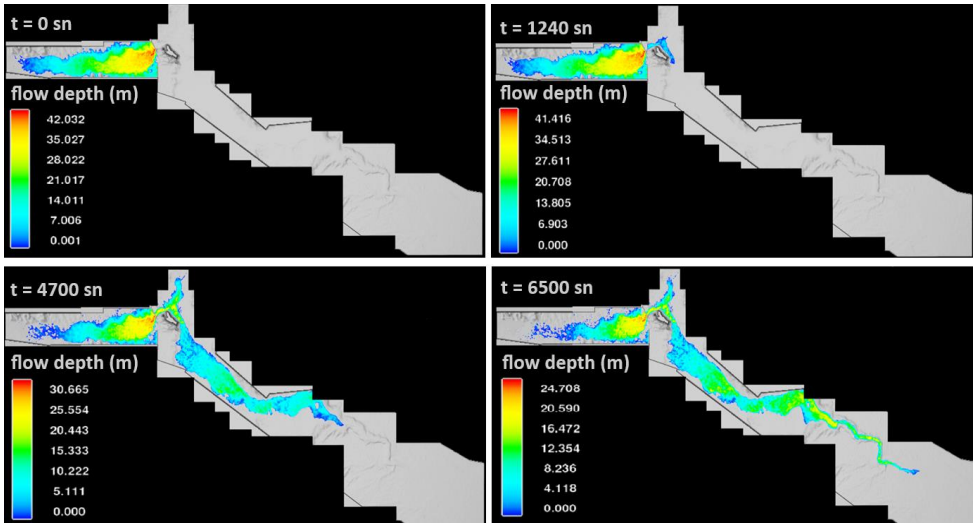

Figure 11. Flood depths and propagation over time for Scenario 3 in 2D analyses in Flow3D.

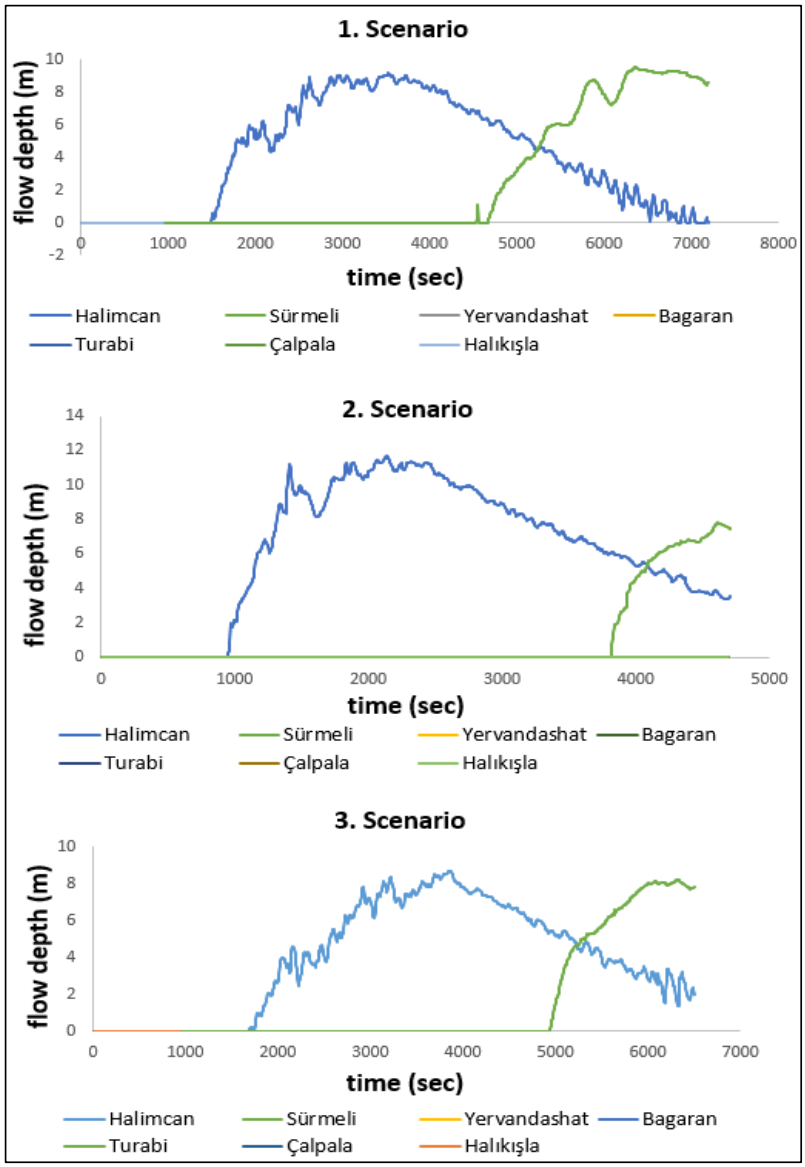

Figure 12. Flow depths in settlements for Scenarios 1, 2, and 3 in 2D analyses in Flow3D.

When the 2D dam failure simulation results were examined, it was seen that Halimcan village, located approximately 1.6 km from the dam axis, experienced maximum water depths of 9.12 m, 11.26 m, and 8.68 m for Scenarios 1, 2, and 3, respectively. In Surmeli village, located approximately 15 km from the dam axis, maximum water depths of 9.61 m, 8.15 m, and 8.20 m were observed for Scenarios 1, 2, and 3, respectively. Additionally, the arrival times of floodwaters at Halimcan village were observed to be 24 min, 16 min, and 28 min for Scenarios 1, 2, and 3, respectively, while for Surmeli village, the corresponding times were 75 min, 62 min, and 82 min (Figure 12).

The changes in the flood propagation and flow depths over time for each scenario in the 3D analyses are shown in the Figures 13–15, below.

Similar to the 2D simulation results, only the Halimcan and Surmeli villages were affected by the flood waves. The flood depths in the village settlements for each scenario in the 3D analysis are shown in Figure 16.

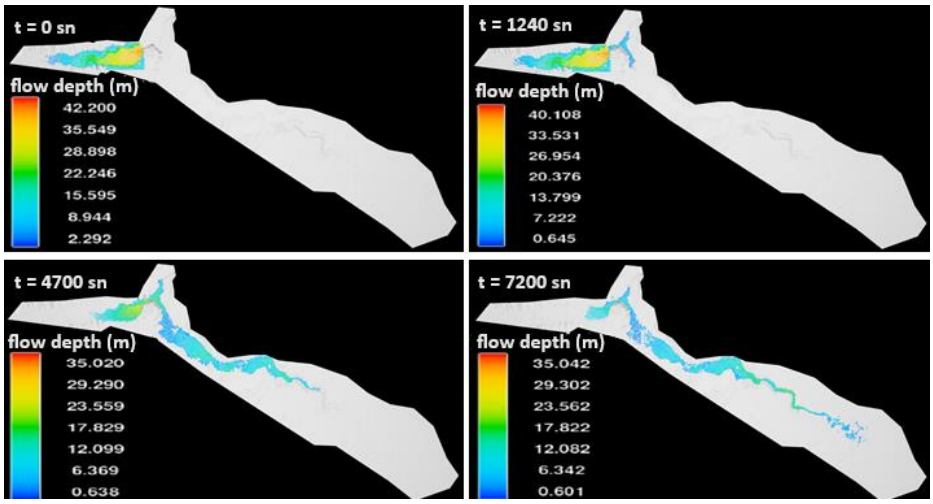

Figure 13. Flood depths and propagation over time for Scenario 1 in 3D analyses in Flow3D.

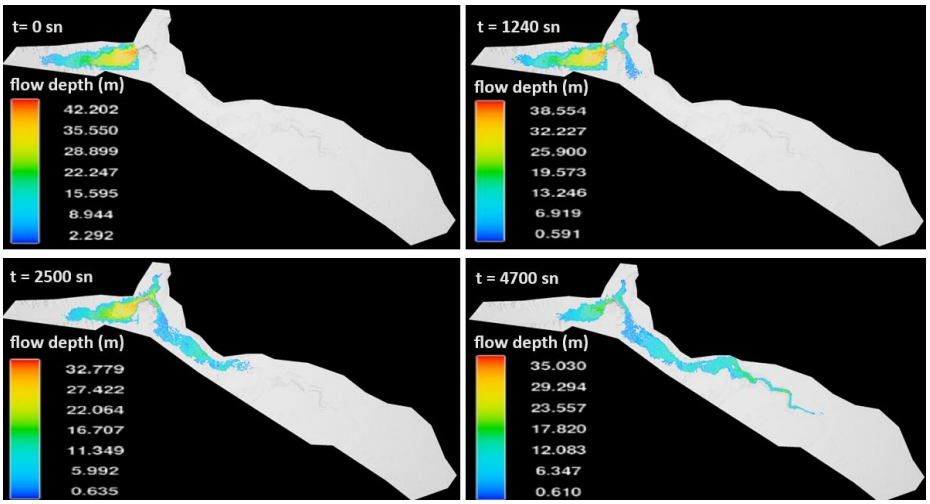

Figure 14. Flood depths and propagation over time for Scenario 2 in 3D analyses in Flow3D.

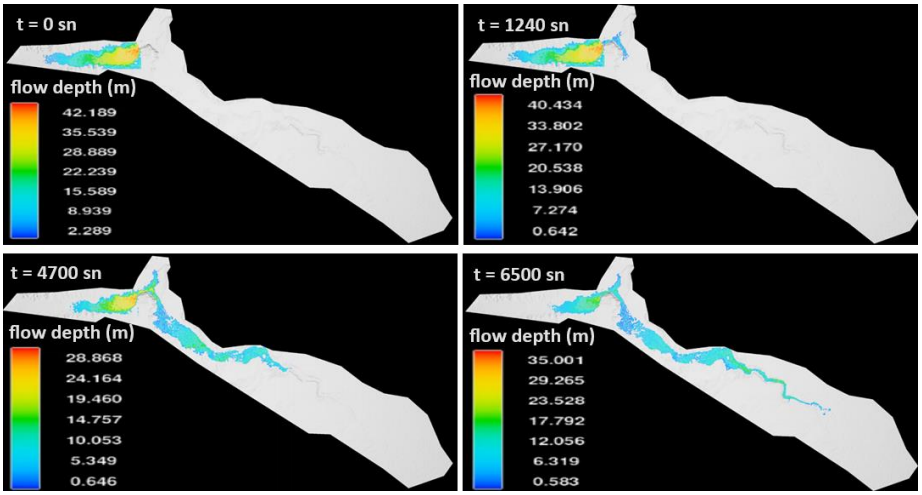

Figure 15. Flood depths and propagation over time for Scenario 3 in 3D analyses in Flow3D.

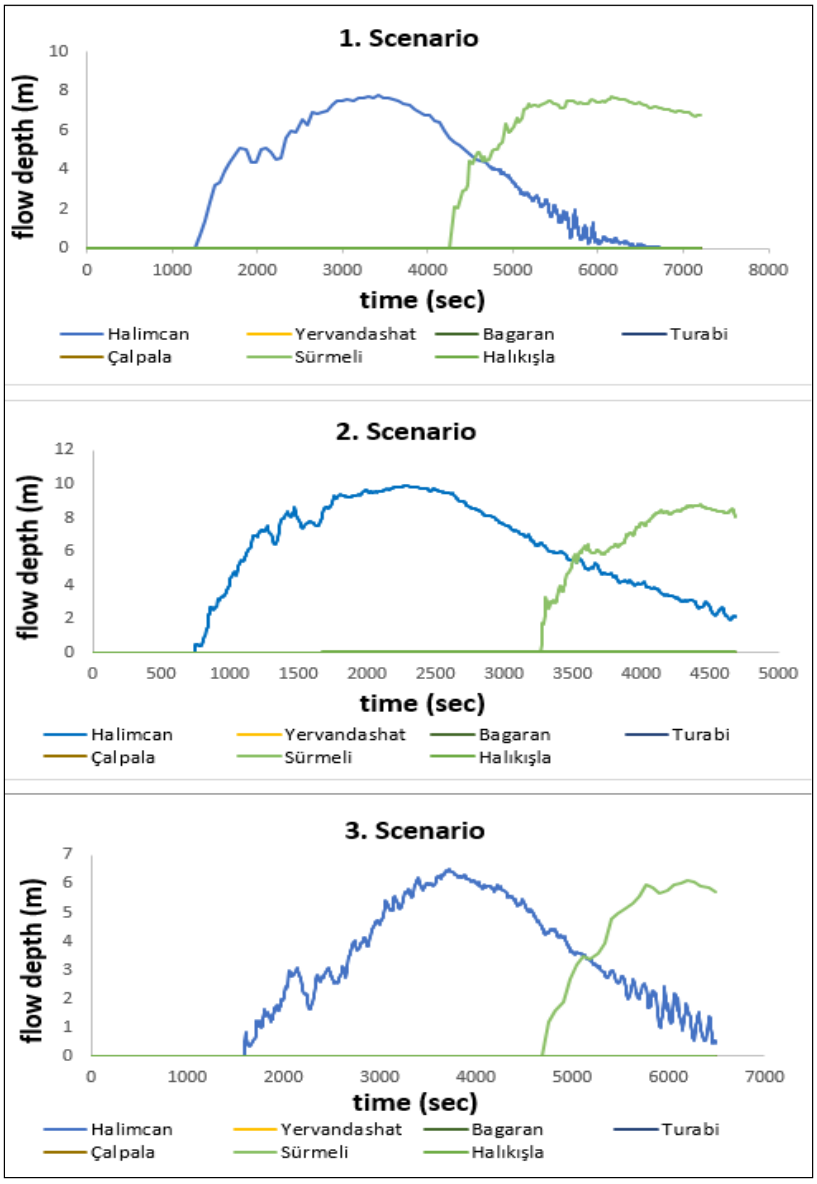

Figure 16. Flow depths in settlements for Scenarios 1, 2, and 3 in 3D analyses in Flow3D.

When the 3D dam failure simulation results were examined, it was seen that Halimcan village experienced maximum water depths of 7.8 m, 9.9 m, and 6.45 m for Scenarios 1, 2, and 3, respectively. In Surmeli village, maximum water depths of 7.6 m, 8.9 m, and 6.1 m were observed for Scenarios 1, 2, and 3, respectively. Additionally, the arrival times of floodwaters at Halimcan village were observed to be 22 min, 13 min, and 26 min for Scenarios 1, 2, and 3, respectively, while for Surmeli village, the corresponding times were 71 min, 54 min, and 79 min.

In order to obtain the flood hydrographs that would occur at the dam axis, a Flux Surface was placed at the dam axis in Flow3D. The flood hydrographs obtained in the 2D and 3D analyses for all scenarios are shown in Figure 17.

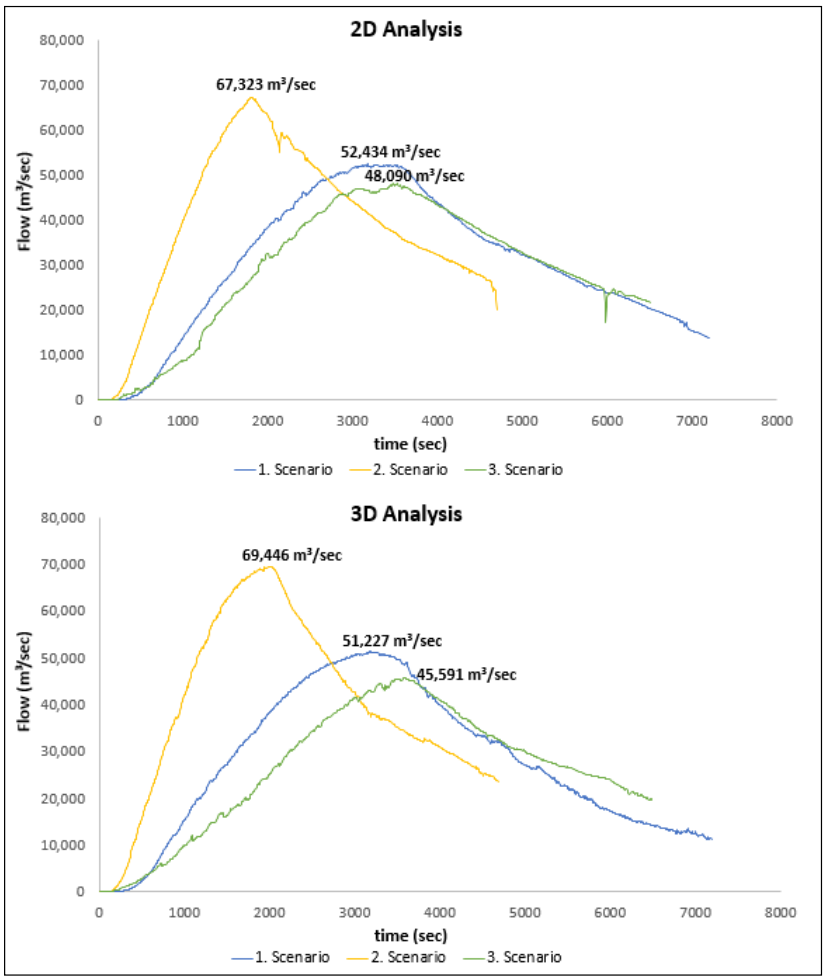

Figure 17. The flood hydrographs on the dam axis for Scenarios 1, 2, 3 in 2D and 3D Analyses.

In the conducted 2D and 3D simulations, it was observed that the highest peak discharge occurred in Scenario 2, which had a shorter failure time, while the lowest peak discharge occurred in Scenario 3, which had the smallest breach cross-sectional area.

The peak discharges for Scenarios 1, 2, and 3 in the 2D simulation were 52,434 m^3/s, 67,323 m^3/s, and 48,090 m^3/s, respectively. The times taken to reach the peak discharge were observed as 3175 s, 1805 s, and 3529 s, respectively. The peak discharges for Scenarios 1, 2, and 3 in the 3D simulation were 51,227 m^3/s, 69,446 m^3/s, and 45,591 m^3/s, respectively. The times taken to reach the peak discharge were observed as 3262 s, 2025 s, and 3578 s, respectively (Figure 17).

For the results of the 2D analysis, when the effect of the failure time on the propagation of the flood was examined in Scenarios 1 and 2 with the same breach geometry, in Scenario 2 (30 min), where the failure time is shorter, the peak flow value was 28% higher. This

situation is also compatible with the study conducted by Bello et al. [32], in which the failure time was stated as the most important parameter affecting flood propagation in dam failures. When Scenarios 1 and 3 with the same failure time and different breach geometries are compared, it is seen that the peak flow value is 9% lower in the 3rd scenario, where the breach cross sectional area is approximately 30% smaller. It was observed that the results were compatible with similar studies in the literature [10,41,56].

When the peak flows were compared according to the 3D analysis results, it was observed that the peak flow value in the 2nd scenario was 35% larger than the 1st scenario. When Scenarios 1 and 3 are compared, it is seen that the peak flow value is 12% lower in the 3rd scenario. It was observed that the results were compatible with similar studies in the literature [10,41,56].

In the validation study, the dam failure experiment performed by Soares-Frazao [24] was solved numerically through 2D and 3D analyses using the Flow3D software, and the results were compared. The simulations performed on a computer with an Intel i7 processor, 6 cores, and 16 GB of RAM took 3 min for the 2D analysis and 30 min for the 3D analysis. The comparison of the water level changes at the G1, G2, and G3 points with the experiment results is shown in Figure 18.

The numerical model demonstrated satisfactory compatibility with the experimental results obtained using both the 2D and 3D methods. The 2D model, which solves the shallow water equations, showed successful results at the G3 point, where there are no obstacles, but it showed a relatively poorer performance at the G2 and G1 points, located downstream of the sill. It has been observed that 3D analysis, which solves using Navier-Stokes equations, is more successful in general, and especially in cases of sudden topographic changes, hydraulic jumps, and the timing of water movement. This observation is consistent with the studies that involve similar comparisons in the literature [33,39,57–60].

To determine the amount of deviation between the experimentally determined water depths and those obtained from the numerical simulations, the Root Mean Square Error (*RMSE*) has been calculated for three probe points. The results are presented in Table 4.

$$RMSE = \sqrt{\frac{1}{n}\sum_{i=1}^{n}(x - x_i)^2} \quad (4)$$

Table 4. RMSE Values.

Probe	*RMSE* (m)	
	3D	**2D**
G3	0.0047	0.0048
G2	0.0050	0.0051
G1	0.0048	0.0050

To summarize, Figures 9–11 and Figures 13–15, respectively, depict the flood propagation after the dam failure for the 2D and 3D models. Upon examination of the figures, it has been observed that there is no significant difference between the results of the two different solutions. When the risk assessment of the settlements in the downstream area is considered, as seen in Figures 12 and 16, only the Halimcan and Surmeli settlements are affected by the floodwaters in both models. Although there is a slight difference in the water depth of a few meters between the 2D and 3D model results in the settlements, there is a general similarity in the study area. Figure 17 shows the hydrographs obtained at the dam axis for both methods. It can be observed that the peak discharge and time to reach the peak discharge of the hydrographs obtained using the 2D and 3D models are very close to each other, with a difference of approximately 3–5%.

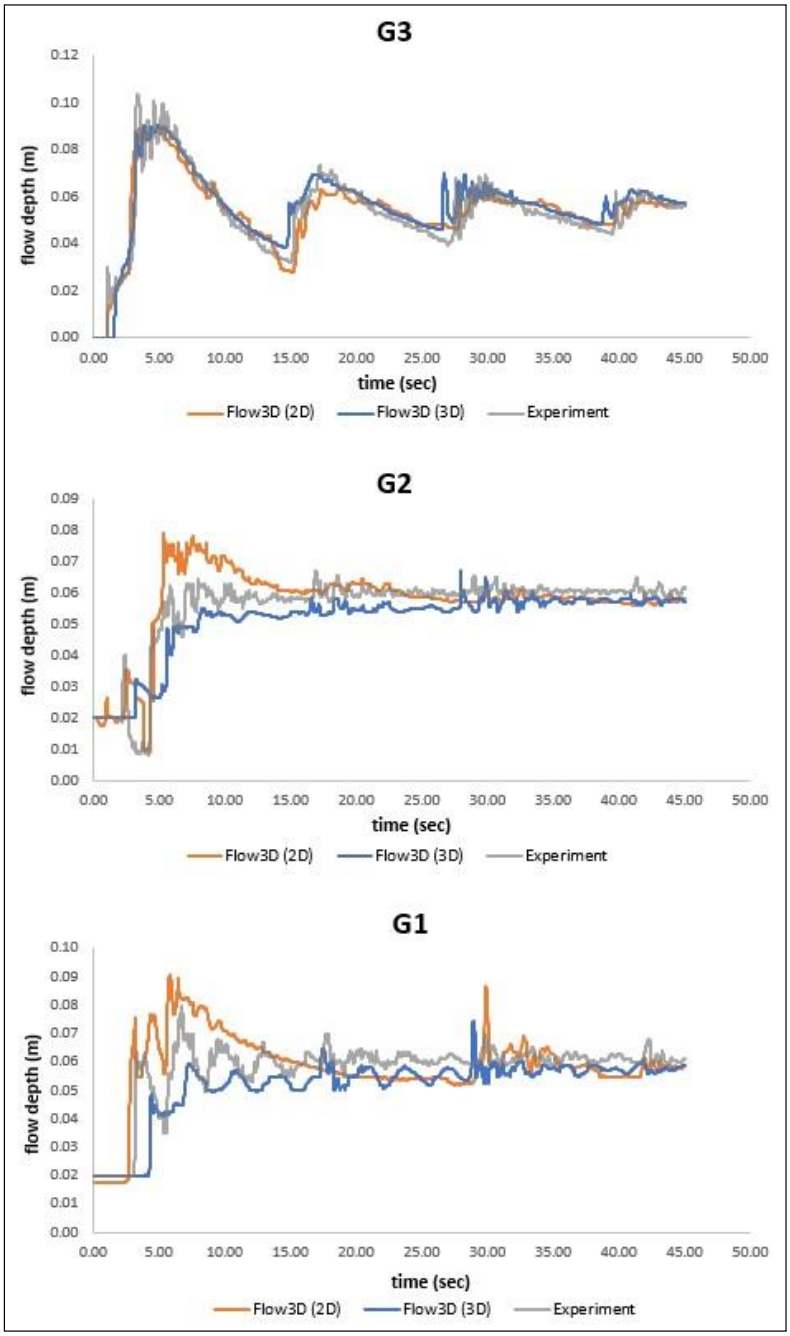

Figure 18. Comparison of experimental and numerical models.

Although 3D models are more successful than 2D models when compared to experimental studies, they have a significant disadvantage at the time point, so much so that in the analyses conducted within the scope of this study, the solution time of the 3D model was about 15 days (357 h), while the solution of the 2D model took 18 h. In this regard, it is thought that 2D modelling may be more useful for large-scale work areas. This situation was stated in studies comparing 2D and 3D numerical solutions of the dam failure experimental setup [36,39].

Within the scope of this study, the mortality rates in the different dam breach scenarios of the Tuzluca Dam were also investigated. In the literature, several methods have been developed to estimate the potential casualties resulting from dam failures (Dekay and McClelland [61], Graham [62], Jonkman [63]). These methods are empirical formulas developed through regression analyses based on data from past dam failures.

In this study, a modified Graham method, which is based on flood simulations, contains more parameters compared to the other methods used. This method is widely used in China, where many dam failures have occurred in the past [64,65].

According to this method, the number of casualties is calculated as follows:

$$L_{OL} = Par.\ f.\ a \tag{5}$$

In these equations, L_{OL} represents loss of life, Par represents people at risk, f represents the fatality rate, and a represents the flood severity coefficient.

$$a = m_1 + bm_2 \tag{6}$$

$$m_1 = \sum_{i=1}^{4} s_i \theta_i \tag{7}$$

$$m_2 = \sum_{i=1}^{9} n_i t_i \tag{8}$$

In these equations, the b and f coefficients are suggested to be 0.25 and 0.75, respectively [62,65–67]. S_i and n_i, used in calculating the m_1 and m_2 values, indicate the value of the factors affecting the loss of life; the expressions θ_i and t_i represent the degree of influence of the factors in question.

The s_1, s_2, s_3, and s_4 values used in calculating the m_1 value are values depending on the population at risk, flood severity, warning time, and local people's awareness about dam failures, respectively. The information regarding these values is given in Table 5. The values of θ_1, θ_2, θ_3, and θ_4 show the degree of effect of the values of s_1, s_2, s_3, and s_4, respectively. The values in question were determined as $\theta_1 = \theta_2 = 0.2$ and $\theta_3 = \theta_4 = 0.3$ according to the Analytical Hierarchy Process (AHP), which is one of the multi-criteria decision-making methods widely used in the literature [65].

Table 5. Suggested ranges of s_i values [65].

s_i	Population at Risk (Person)	Flood Severity	Warning Time (h)	Local People's Awareness about Dam Failures
0.80–1.00	$>10^5$	Extremely high	$W_t < 0.25$	Extremely unclear
0.60–0.80	10^4–10^5	High	$0.25 < W_t < 0.50$	Unclear
0.40–0.60	10^3–10^4	Middle	$0.50 < W_t < 0.75$	Generally clear
0.20–0.40	10^2–10^3	Low	$0.75 < W_t < 1.00$	Clear
0.01–0.20	1–10^2	Extremely low	$W_t > 1.00$	Extremely clear

The n_1, n_2, n_3, n_4, n_5, n_6, n_7, n_8, and n_9 values used in calculating the m_2 value represent, respectively, the young population rate, weather conditions, the time of dam failure, distance to the dam, evacuation and rescue capability, dam height, storage capacity, downstream slope, and building abrasion resistance. The information regarding these values is given in Table 6. Similarly, t_1, t_2, t_3, t_4, t_5, t_6, t_7, t_8, and t_9 indicate the degree of influence of the values n_1, n_2, n_3, n_4, n_5, n_6, n_7, n_8, and n_9, respectively. According to the Analytical Hierarchy Process (AHP) method, these values were determined as $t_1 = t_3 = t_4 = 0.2$, $t_2 = t_5 = 0.1$, and $t_6 = t_7 = t_8 = t_9 = 0.05$ [65].

Table 6. Suggested ranges of n_i values [65].

N_i	0.80–1.00	0.60–0.80	0.40–0.60	0.20–0.40	0.01–0.20
Young population rate (%)	0–20	20–40	40–60	60–80	80–100
Weather conditions	Heavy storm	Rainstorm	Moderate rain	Sprinkle	Sunny days
Time of dam failure	Holiday in the morning	Working day in the morning	Holiday at night	Working days at night	Daytime
Distance to the dam (km)	0–5	5–10	10–20	20–50	>50
Evacuation and rescue capability	Very unsuccessful	Unsuccessful	General	Successful	Very successful
Dam height (m)	>70	30–70	15–30	10–15	<10
Reservoir capacity	Very Large	Large	Medium	Small	Very Small
Downstream slope	Valley	Mountain	Hill	Plain	Beach
Building abrasion resistance	Extremely weak	Weak	Middle	Strong	Extremely strong

The s_i and n_i values were determined by taking into account the 3D analysis results on the basis of the location and scenario. The results are presented in Tables 7 and 8.

Table 7. s_i values selected according to settlement and simulation scenarios.

s_i	Halimcan			Sürmeli		
	1. Scenario	**2. Scenario**	**3. Scenario**	**1. Scenario**	**2. Scenario**	**3. Scenario**
s_1	0.10	0.10	0.10	0.30	0.30	0.30
s_2	0.60	0.80	0.50	0.60	0.80	0.50
s_3	0.70	0.90	0.65	0.10	0.20	0.05
s_4	0.70	0.70	0.70	0.70	0.70	0.70

Table 8. n_i values selected according to settlement and simulation scenarios.

n_i	Halimcan	Sürmeli
	1., 2. and 3. Scenarios	**1., 2. and 3. Scenarios**
n_1	0.50	0.50
n_2	0.40	0.40
n_3	0.50	0.50
n_4	0.90	0.50
n_5	0.40	0.40
n_6	0.65	0.65
n_7	0.60	0.60
n_8	0.80	0.90
n_9	0.80	0.80

Note(s): n_i values are the same on a scenario-by-scenario basis as they include social and environmental factors.

Using the data in Tables 7 and 8 and Equations (5)–(8), the possible casualties were calculated according to the settlements and scenarios in the event of the failure of the Tuzluca Dam.

The estimated casualties for the settlements of Halimcan, with a population of 41, and Surmeli, with a population of 434, are presented in Table 9.

Table 9. Projected loss of life in the event of Tuzluca Dam failure.

	Halimcan L_{OL} (Person)	**Sürmeli L_{OL} (Person)**	**Total L_{OL} (Person)**
1. Scenario	22	179	201
2. Scenario	25	202	227
3. Scenario	21	170	191

When Table 9 is examined, it is seen that there will be serious losses of life in the case of the possible collapse of the Tuzluca Dam. In Halimcan village, which is close to the dam

axis (1.6 km), it is expected that 54%, 61%, and 51% of the population will lose their lives in the 1st, 2nd, and 3rd scenarios, respectively. In Surmeli village, which is approximately 15 km away from the dam axis, it is expected that 41%, 47%, and 39% of the population will lose their lives in the 1st, 2nd, and 3rd scenarios, respectively. The total losses of life was 13% higher in Scenario 2 (30 min), where the failure time was shorter, than in Scenario 1 with the same breach geometry. When Scenarios 1 and 3, with the same failure time and different breach geometries, are compared, it is seen that total loss of life is 5% lower in the 3rd scenario, where the breach cross sectional area is approximately 30% smaller. This shows that the dam failure time and breach geometry have an impact on the loss of life that may occur.

4. Conclusions

In this study, 2D and 3D dam-break simulations of the Tuzluca Dam, planned for the Igdir province in Turkey, were conducted using the Flow3D software. The same computer was used in all simulations. The propagation of flood waves was investigated under three different scenarios based on the breach geometry, failure type, and failure times. To validate the numerical model, the dam-break experiment conducted by Soares-Frazao [24] was numerically simulated using the Flow3D software. While both numerical models (2D and 3D) exhibited sufficient compatibility with the experimental results, the 3D analysis was more successful in this regard. In the dam failure simulations of the case study, although the 2D and 3D models provided similar results, the 3D analysis required approximately 20 times more computation time compared to the 2D analysis. Consequently, it has been concluded that for extensive studies like dam failures, 2D analyses may be more practical. For smaller-scale scenarios or situations necessitating higher precision, 3D modelling is deemed suitable. Additionally, if high-performance computers with 32 or 64 cores are accessible, the computation time for dam failure simulations employing 3D analysis can be mitigated.

In addition, the possible loss of life was estimated within the scope of the study, and it was seen that serious loss of life could occur in the Halimcan and Sürmeli villages. The analyses revealed that the breach geometry, especially the dam failure time, has a significant impact on the flood propagation and potential loss of life. The information obtained regarding the flood hydrographs, flood depths in the settlements, and the time it takes for the flood to reach the settlements offers valuable insights into the failure scenario of the Tuzluca Dam. It is believed that the obtained information will guide the preparation of disaster and emergency action plans for the region. For example, the settlement of Halimcan, located approximately 1.6 km downstream of the dam axis and experiencing significant flood depths in all scenarios, has not been included in the resettlement plan prepared by the government. Due to the low population in Halimcan (41), taking the action to include it in a resettlement plan at a reasonable cost could be a measure to reduce the risk in the region. Another example would be the village of Surmeli, with a population of 434, located approximately 15 km downstream of the dam axis, where serious flood depths occur in all scenarios. Various measures are proposed to mitigate the potential damage to settlements in the event of a dam failure. These measures include increasing the existing vegetation in the study area, installing audible and visual warning systems to provide rapid and effective information to the public in the event of a dam failure, educating the local population about the risk of dam failure, and appropriate response procedures. It is also recommended to construct cost-effective small-scale water retention facilities in certain areas and apply soil conservation techniques to increase water absorption.

In the literature, dam-break simulations have been conducted for either existing or collapsed dams. Considering past dam breaks and their adverse effects, dam-break analyses should be conducted for planning-stage dams, similar to this study, to identify the necessary risk conditions before dam construction and integrate them into resettlement and emergency action plans. Additionally, similar studies can be carried out using different

CFD software (Fluent, Mike3D, Openfoam, etc.) as an alternative to Flow3D, and the results can be compared.

Author Contributions: Conceptualization, C.A. and S.S.N.; software, C.A. and A.U.; analysis, C.A.; writing—original draft preparation, review, and editing, C.A., S.S.N. and A.U. All authors have read and agreed to the published version of the manuscript.

Funding: This study was supported by the Scientific Research Projects Coordination Unit of Gumushane University (Grant number: 21.F5110.02.01).

Data Availability Statement: Data sharing is not applicable to this article.

Conflicts of Interest: The authors declare no conflict of interest.

References

1. Viseu, T.; de Almeida, A.B. Dam-break risk management and hazard mitigation. *State Art Sci. Eng.* **2009**, *36*, 211–239.
2. Xiong, Y. Dam break analysis using HEC-RAS. *J. Water Resour. Prot.* **2011**, *3*, 370–379. [CrossRef]
3. Le, T.T.H.; Nguyen, V.C. Numerical study of partial dam–break flow with arbitrary dam gate location using VOF method. *Appl. Sci.* **2022**, *12*, 3884. [CrossRef]
4. Adamo, N.; Al-Ansari, N.; Sissakian, V.; Laue, J. Dam safety and overtopping. *J. Earth Sci. Geotech. Eng.* **2020**, *10*, 41–78.
5. Lumbroso, D.; Davison, M.; Body, R.; Petkovšek, G. Modelling the Brumadinho tailings dam failure, the subsequent loss of life and how it could have been reduced. *Nat. Hazards Earth Syst. Sci.* **2021**, *21*, 21–37. [CrossRef]
6. Froehlich, D.C. Embankment Dam breach parameters and their uncertainties. *J. Hydraul. Eng.* **2008**, *134*, 1708–1721. [CrossRef]
7. Najar, M.; Gül, A. Investigating the influence of dam-breach parameters on dam-break connected flood hydrograph. *Tech. J.* **2022**, *33*, 12501–12524. [CrossRef]
8. International Commission onLarge Dams. *Dam Failures—Statistical Analysis*; Bulletin No. 99; International Commission on Large Dams: Paris, France, 1995.
9. MacDonald, T.C.; Langridge-Monopolis, J. Breaching characteristics of dam failures. *J. Hydraul. Eng.* **1984**, *110*, 567–586. [CrossRef]
10. Karakaya, K. Numerical Simulation of the Kirazliköprü Dam Failure on the Gökırmak River. Master's Thesis, Middle East Technical University, Ankara, Turkey, 2005.
11. Wu, W. *Introduction to DLBreach—A Simplified Physically-Based Dam/Levee Breach Model*; Technical Report; Clarkson University: Potsdam, NY, USA, 2016.
12. Ackerman, C.T.; Brunner, G.W. Dam failure analysis using HEC-RAS and HEC-GEORAS. In Proceedings of the 2008 World Environmental and Water Resources Congress, Ahupua'a, Honolulu, HI, USA, 12–16 May 2008.
13. Li, W.; Zhu, J.; Fu, L.; Zhu, Q.; Xie, Y.; Hu, Y. An augmented representation method of debris flow scenes to improve public perception. *Int. J. Geogr. Inf. Sci.* **2021**, *35*, 1521–1544. [CrossRef]
14. Liu, Z.; Xu, J.; Liu, M.; Yin, Z.; Liu, X.; Yin, L.; Zheng, W. Remote sensing and geostatistics in urban water-resource monitoring: A review. *Mar. Freshw. Res.* **2023**, *74*, 747–765. [CrossRef]
15. Oborie, E.; Rowland, D.R. Flood influence using GIS and remote sensing based morphometric parameters: A case study in Niger delta region. *J. Asian Sci. Res.* **2023**, *13*, 1–15. [CrossRef]
16. Von Thun, J.L.; Gillette, D.R. *Guidance on Breach Parameters*; Internal Memorandum Rep.; U.S. Department of the Interior, Bureau of Reclamation: Denver, CO, USA, 1990.
17. Froehlich, D.C. Embankment dam breach parameters revisited. In Proceedings of the First International Conference on Water Resources Engineering, San Antonio, TX, USA, 14–18 August 1995; American Society of Civil Engineers: New York, NY, USA, 1995; pp. 887–891.
18. Xu, Y.; Zhang, L.M. Breaching parameters for earth and rockfill dams. *J. Geotech. Geoenviron. Eng.* **2009**, *135*, 1957–1970. [CrossRef]
19. Khoshkonesh, A.; Nsom, B.; Bahmanpouri, F.; Dehrashid, F.A.; Adeli, A. Numerical study of the dynamics and structure of a partial dam-break flow using the VOF method. *Water Resour. Manag.* **2021**, *35*, 1513–1528. [CrossRef]
20. Aureli, F.; Maranzoni, A.; Petaccia, G.; Soares-Frazão, S. Review of experimental investigations of dam-break flows over fixed bottom. *Water* **2023**, *15*, 1229. [CrossRef]
21. Bella, S.W.; Elliot, R.C.; Chaudry, M.H. Experimental results of two dimensional dam-break flows. *J. Hydraul. Res.* **1992**, *30*, 225–252. [CrossRef]
22. Lauber, G.; Hager, W.H. Ritter's dambreak wave wevisited. In Proceedings of the 27 IAHR Congress, San Francisco, CA, USA, 10–15 August 1997; pp. 258–262.
23. Ritter, A. Die fortpflanzung de wasserwellen. *Z. Ver. Dtsch. Ingenieure* **1892**, *36*, 947–954. (In German)
24. Soares-Frazão, S. Experiments of dam-break wave over a triangular bottom sill. *J. Hydraul. Res.* **2007**, *45*, 19–26. [CrossRef]
25. Hui, L.; Liu, H.; Guo, L.; Lu, S. Experimental study on the dam-break hydrographs at the gate location. *J. Ocean. Univ. China* **2017**, *16*, 697–702.
26. Stoker, J.J. *Water Waves*; Interscience Publishers Inc.: Hoboken, NJ, USA, 1957.

27. Lin, B.; Gong, Z.; Wang, L. Dam-site hydrographs due to sudden release. *Sci. Sin.* **1980**, *23*, 1570–1582.
28. Quecedo, M.; Pastor, M.; Herreros, M.I.; Merodo, J.A.F.; Zhang, Q. Comparison of two mathematical models for solving the dam break problem using the FEM method. *Comput. Methods Appl. Mech. Engrg.* **2005**, *194*, 3984–4005. [CrossRef]
29. Albano, R.; Mancusi, L.; Adamowski, J.; Cantisani, A.; Sole, A. A GIS tool for mapping dam-break flood hazards in Italy. *ISPRS Int. J. Geo-Inf.* **2019**, *8*, 250. [CrossRef]
30. Říha, J.; Kotaška, S.; Petrula, L. Dam break modeling in a cascade of small earthen dams: Case study of the Cižina River in the Czech Republic. *Water* **2020**, *12*, 2309. [CrossRef]
31. Psomiadis, E.; Tomanis, L.; Kavvadias, A.; Soulis, K.X.; Charizopoulos, N.; Michas, S. Potential dam breach analysis and flood wave risk assessment using HEC-RAS and remote sensing data: A multicriteria approach. *Water* **2021**, *13*, 364. [CrossRef]
32. Bello, D.; Alcayaga, H.; Caamaño, D.; Pizarro, A. Influence of dam breach parameter statistical definition on resulting rupture maximum discharge. *Water* **2022**, *14*, 1776. [CrossRef]
33. Kocaman, S. Experimental and Theoretical İnvestigation of Dam Break Problem. Ph.D. Thesis, Department of Civil Engineering Institute of Natural and Applied Sciences University of Çukurova, Adana, Türkiye, 2007.
34. Vasquez, J.A. Testing River2D and Flow3D for sudden dam-break flow simulations. In Proceedings of the Conference on Canadian Dam Association, Whistler, BC, Canada, 3–8 October 2009.
35. Larocque, L.A.; Imran, J.; Chaudhry, M.H. 3D numerical simulation of partial breach dam break flow using the LES and k–ε turbulence models. *J. Hydraul. Res.* **2013**, *51*, 145–157. [CrossRef]
36. Robb, D.M.; Vasquez, J.A. Numerical simulation of dam–break flows using depth-averaged hydrodynamic and three-dimensional CFD models. In Proceedings of the 22nd Canadian Hydrotechnical Conference, Montreal, QC, Canada, 29 April–2 May 2015.
37. Tahershamsi, A.; Hooshyaripor, F.; Razib, S. Reservoir's geometry impact of three dimensions on peak discharge of dam-failure flash flood. *Sci. Iran.* **2017**, *25*, 1931–1942. [CrossRef]
38. Franco, A.; Moernaut, J.; Schneider-Muntau, B.; Strasser, M.; Gems, B. The 1958 Lituya Bay tsunami–prevent bathymetry reconstruction and 3D numerical modelling utilising the computational fluid dynamics software Flow-3D. *Nat. Hazards Earth Syst. Sci.* **2020**, *20*, 2255–2279. [CrossRef]
39. Kocaman, S.; Evangelista, S.; Guzel, H.; Dal, K.; Yilmaz, A.; Viccione, G. Experimental and numerical investigation of 3D dam-break wave propagation in an enclosed domain with dry and wet bottom. *Appl. Sci.* **2021**, *11*, 5638. [CrossRef]
40. Republic of Turkey General Directorate of Electricity Works and Studies. Feasibility Report of the Lower Aras Basin Tuzluca Dam and HEPP Project, 2004.
41. Bharath, A.; Shivapur, A.V.; Hiremath, C.G.; Maddamsetty, R. Dam break analysis using HEC-RAS and HEC-GeoRAS: A case study of Hidkal dam, Karnataka state, India. *Environ. Chall.* **2021**, *5*, 100401. [CrossRef]
42. Annis, A.; Nardi, F.; Petroselli, A.; Apollonio, C.; Arcangeletti, E.; Tauro, F.; Belli, C.; Bianconi, R.; Grimaldi, S. UAV-DEMs for small-scale flood hazard mapping. *Water* **2020**, *12*, 1717. [CrossRef]
43. Sena, N.C.; Veloso, G.V.; Fernandes-Filho, E.I.; Francelino, M.R.; Schaefer, C.E.G. Analysis of terrain attributes in different spatial resolutions for digital soil mapping application in southeastern Brazil. *Geoderma Reg.* **2020**, *21*, e00268. [CrossRef]
44. Khojeh, S.; Ataie-Ashtiani, B.; Hosseini, S.M. Effect of DEM resolution in flood modeling: A case study of Gorganrood River, Northeastern Iran. *Nat. Hazards* **2022**, *112*, 2673–2693. [CrossRef]
45. Uysal, G.; Tasci, E. Analysis of downstream flood risk in the failure of Batman Dam with two-dimensional hydraulic modeling and satellite data. *J. Nat. Hazards Environ.* **2023**, *9*, 39–57.
46. USBR. *Downstream Hazard Classification Guidelines*; ACER Tech. Memorandum Rep. No. 11; U.S. Department of the Interior, Bureau of Reclamation: Denver, CO, USA, 1988.
47. Yin, Y.P.; Huang, B.L.; Chen, X.T.; Liu, G.N.; Wang, S.C. Numerical analysis of wave generated by the Qianjiangping landslide in three Gorges Reservoir. *J. Int. Consort. Landslides* **2015**, *12*, 355–364. [CrossRef]
48. Flow Science Inc. *Flow-3D Version 10.0 User's Manual*; Flow Science Inc.: Santa Fe, New Mexico, 2007.
49. Tannehill, J.C.; Anderson, D.A.; Pletcher, R.H. *Computational Fluid Mechanics and Heat Transfer*, 2nd ed.; Taylor & Francis: New York, NY, USA, 1997; p. 792.
50. Kaheh, M.; Kashefipour, M.A.; Dehghani, A.A. Comparison of k-ε and RNG k-ε turbulent models for estimation of velocity profiles along the hydraulic jump on corrugated beds. In Proceedings of the 6th International Symposium on Environmental Hydraulics, Athens, Greece, 23–25 June 2010.
51. Dehdar-behbahani, S.; Parsaie, A. Numerical modeling of flow pattern in dam spillway's guide wall. Case study: Balaroud dam, Iran. *Alex. Eng. J.* **2016**, *55*, 467–473. [CrossRef]
52. Oliva, J.B.; Valentin, M.G. Comparative Evaluation of Two Different 3D OpenFOAM Modules in a Dam-Break Test. Bachelor's Thesis, Higher Technical School of Road, Canals Engineering, Barcelona, Spain, 2017.
53. Ersoy, H.; Karahan, M.; Gelişli, K.; Akgun, A.; Anılan, T.; Sunnetci, M.O.; Yahsi, B.K. Modelling of the landslide-induced impulse waves in the Artvin Dam reservoir by empirical approach and 3D numerical simulation. *Eng. Geol.* **2019**, *249*, 112–128. [CrossRef]
54. Karahan, M.; Ersoy, H.; Akgun, A. A 3D numerical simulation-based methodology for Assessment of landslide-generated impulse waves: A case study of the Tersun Dam reservoir (NE Turkey). *J. Int. Consort. Landslides* **2020**, *17*, 2777–2794. [CrossRef]
55. Aksoy, A.O.; Dogan, M.; Guven, S.O.; Tanır, G.; Guney, M.S. Experimental and numerical investigation of the flood waves due to partial dam break. *Iran. J. Sci. Technol. Trans. Civ. Eng.* **2022**, *46*, 4689–4704. [CrossRef]

56. Shahrim, M.F.; Ros, F.C. Estimation of breach outflow hydrograph using selected regression breach equations. In *IOP Conference Series: Earth and Environmental Science*; IOP Publishing: Bristol, UK, 2020; p. 476.
57. Hien, L.T.H.; Nguyen, V.C. Investigate Impact Force of Dam-Break Flow against Structures by Both 2D and 3D Numerical Simulations. *Water* **2021**, *13*, 344. [CrossRef]
58. Zhang, T.; Peng, L.; Feng, P. Evaluation of a 3D unstructured-mesh finite element model for dam-break flood. *Comput. Fluids* **2018**, *160*, 64–77. [CrossRef]
59. Dai, S.; He, Y.; Yang, J.; Ma, Y.; Jin, S.; Liang, C. Numerical study of cascading dam- break characteristics using SWEs and RANS. *Water Supply* **2020**, *20*, 348–360. [CrossRef]
60. Ozmen-Cagatay, H.; Kocaman, S. Dam-break flows during initial stage using SWE and RANS approaches. *J. Hydraul. Res.* **2010**, *48*, 603–611. [CrossRef]
61. DeKay, M.L.; McClelland, G.H. Predicting loss of life in cases of dam failure and flash flood. *Risk Anal.* **1993**, *13*, 193–205. [CrossRef]
62. Graham, W.J. A procedure for estimating loss of life caused by dam failure. *Sediment River Hydral.* **1999**, *6*, 1–43.
63. Jonkman, S.N. Loss of Life Estimation in Flood Risk Assessment. Ph.D. Thesis, Delft University, Delft, The Netherlands, 2007.
64. Xiaoling, W.; Xuefei, A.; Ruirui, S.; Weiping, G. The comprehensive risk analysis of dam-break consequences based on Numerical Simulation. *Appl. Mech. Mater.* **2012**, *229*, 1850–1853.
65. Sun, R.; Wang, X.; Zhou, Z.; Ao, X.; Sun, X.; Song, M. Study of the comprehensive risk analysis of dam-break flooding based on the numerical simulation of flood routing. Part I: Model development. *Nat. Hazards* **2014**, *73*, 1547–1568. [CrossRef]
66. Sun, R.; Wang, X.; Zhou, Z.; Ao, X.; Sun, X.; Song, M. Study of the comprehensive risk analysis of dam-break flooding based on the numerical simulation of flood routing. Part II: Model application and results. *Nat. Hazards* **2014**, *72*, 675–700.
67. Zhou, K.F. Study on Analysis Method for Loss of Life Due to Dam Breach. Master's Thesis, Nanjing Hydraulic Research Institute, Nanjing, China, 2006.